# Dynamics of Hydration Water Around Native and Misfolded $\alpha$-Lactalbumin

Z. F. Brotzakis,[†] C. C. M. Groot,[‡] W. H. Brandeburgo,[†] H. J. Bakker ,[‡] and P. G. Bolhuis[*,†]

*Van 't Hoff Institute for Molecular Sciences, Universiteit van Amsterdam, Science Park 904, 1098 XH Amsterdam, The Netherlands, and FOM Institute AMOLF, Science Park 104, 1098 XG Amsterdam, The Netherlands*

E-mail: p.g.bolhuis@uva.nl

[*]To whom correspondence should be addressed

[†]Van 't Hoff Institute for Molecular Sciences, Universiteit van Amsterdam, Science Park 904, 1098 XH Amsterdam, The Netherlands

[‡]FOM Institute AMOLF, Science Park 104, 1098 XG Amsterdam, The Netherlands

**Abstract**

As water is an essential ingredient in protein structure, dynamics and functioning, knowledge of its behavior near proteins is crucial. We investigate water dynamics around bovine $\alpha$-lactalbumin by combining molecular dynamics simulations with polarization-resolved femtosecond infrared (fs-IR) spectroscopy. We identify slowly reorienting surface waters and establish their hydrogen-bond lifetime and reorientation dynamics, which we compare to the experimentally measured anisotropy decay. The calculated number of slow surface waters is in reasonable agreement with the results of fs-IR experiments. While surface waters form fewer hydrogen bonds than the bulk, within the hydration layer water is slower when donating more hydrogen bonds. At concave sites the protein-water hydrogen bonds break preferably via translational diffusion rather than via a hydrogen-bond jump mechanism. Water molecules reorient slower near these sites than at convex water exposed sites. Protein misfolding leads to an increased exposure of hydrophobic groups, inducing relatively faster surface water dynamics. Nevertheless, the larger exposed surface slows down a larger amount of water. While for native proteins hydrating water is slower near hydrophobic than near hydrophilic residues, mainly due to stronger confinement, misfolding causes hydrophobic water to reorient relatively faster because exposure of hydrophobic groups destroys concave protein cavities with a large excluded volume.

# Introduction

The protein hydration shell is very significant and essential to protein structure, dynamics and function. The hydration shell dynamics relates to biochemical processes such as protein folding, molecular recognition and enzyme function[1–3]. Both experimental[3,4] and simulation findings[5–7] agree on that a protein perturbs the water dynamics in its hydration shell. However, the root and the degree of this perturbation is not completely understood. Experimental techniques such as time-resolved fluorescence and NMR indicate a slowdown of water molecules close to the protein surface. NMR experiments[8], and molecular dynamics

(MD) simulations[5,7], show that most of the hydration shell water reorients 2-3 times slower compared to bulk water. The origin of this slowdown has been mostly attributed to the excluded volume effect due to topology and, to a lesser extent, to the larger strength of the hydrogen bond [5,7].

Moreover, MD simulations[7] indicated that increasing the excluded volume and decreasing the hydration level by adding hexane molecules at the surface, led to shifted and broader reorientation time distributions. The effect of confinement on water dynamics has been assessed experimentally by polarization-resolved femtosecond infrared spectroscopy [9,10], which showed that water near the surface of a (reversed) micelle is slow, while water in the core behaves very similar to bulk water. These experiments showed that confinement affects the dynamics of water, but only on very small length scales (sub nanometer), i.e. close to a surface. Femtosecond 2D infrared spectroscopy combined with polarization-resolved femtosecond infrared spectroscopy[11] showed that the slow component of water reorientation dynamics scales with the slow translational diffusion, indicating slow hydrogen bond dynamics near hydrophobic groups. Interestingly, in a MD study on a amyloidgenic $\alpha\beta$ disordered protein at room temperature, Jose *et al.*[12] found that water molecules around the protein exhibit faster reorientation and translation dynamics compared to water hydrating a native globular ubiquitin in water. Further studies conducted by Rahaman et al[13] observed also an acceleration of water dynamics around a temperature induced-unfolded thermophile protein compared to a folded one. Temperature induced unfolding or misfolding of the proteins alters the amount of confined water, and changes the hydrophobic/hydrophilic nature of the protein surface. The influence of this temperature induced misfolding on the water dynamics remains not well understood. In this work, by combining molecular dynamics simulations with infrared spectroscopy, we investigate the dynamics of water around the protein surface of $\alpha$-lactalbumin, a major constituent of whey, and an important protein in the food industry[14]. As $\alpha$-lactalbumin is a small (14kDa) globular protein that is structurally quite similar to the widely studied lysozyme[15], it forms an excellent system to study water dy-

namics in the protein hydration shell. We conducted MD simulations of several solvated $\alpha$-lactalbumin systems at ambient conditions. For a native solvated protein, we investigated two different concentrations and two different water models. For a misfolded solvated protein we investigated one concentration and one water model. In addition, we measured the water reorientation dynamics using polarization-resolved femtosecond infrared spectroscopy. The remainder of the paper is organized as follows. The next section describes the employed simulation, analysis and experimental methodology. Subsequently, we present and discuss the analysis results, and compare to the experiments. We end with conclusions.

# Methods

## Simulation setup

All molecular dynamics simulations were performed with the Gromacs 4.5.4 package [16]. The bovine $\alpha$-lactalbumin monomer structure, extracted from the PDB 1F6S [17] was solvated with water molecules (SPC/E or TIP4P/2005), resulting in dilute solutions of approximately 5% w/w and more concentrated solutions of 8.5% w/w ( denoted 5 % SPC/E, 5% TIP4P/2005, 8.5% SPC/E and 8.5% TIP4P/2005 system, respectively ) .

The atomic interactions were defined by the amber99sb-ildn force field [18]. The protonation state of the amino acids corresponds to pH of 7, and five Na atoms were added to neutralize the system (pkI= 4-5). For each water force-field, after energy minimization, the system was equilibrated for 1 ns at ambient conditions (298 K and 1 atm) in the NPT ensemble. All bonds were constrained with the Lincs algorithm. A cutoff of 1 nm was used for the non-bonded Lennard-Jones interactions. The Particle Mesh Ewald method was used to calculate the electrostatic interactions with a Fourier spacing of 0.12 nm and a 1 nm cutoff for the short range electrostatic interactions. Neighbor lists were updated every 10 fs with a cutoff of 1 nm and the time step was 2 fs [18]. The leap-frog algorithm was used for integrating Newton's equations of motion. In the NPT simulations the v-rescale thermostat [19] with a

coupling time constant of 0.2 ps controlled the temperature, while the Parrinello-Rahman barostat[20] with a coupling time constant of 1.0 ps kept the pressure constant. From a 100 ns long MD trajectory in the NPT ensemble at ambient conditions (298 K and 1 atm) 10 frames were randomly selected from different parts of the trajectory. From each frame we initiated a short 1 ns production run in the NVE ensemble, by switching off the thermostat and barostat. This approach eliminated any unwanted influence from the thermostat or barostat on the dynamics. To prevent energy drift we used a switching function for the non-bonded interactions from 0.8-1.0 nm. The pair lists were updated every 5 fs with a cutoff of 1.2 nm and the time step was 1 fs. The frequency of the energy calculation was 10 fs, and the frames were saved every 100 fs in order to obtain sufficient data for the analysis.

The effect of protein misfolding on the water dynamics was investigated by analyzing two quenched high temperature systems. Starting from the last frame of the 100 ns ambient condition MD trajectories (for the 5% w/w SPC/E system), we ran another 100 ns at high temperature (700 K) followed by two types of quenching procedures. In the first, five high temperature frames were selected and relaxed at 298 K temperature (NPT) for 10 ns. Then, for each of these five room temperature MD runs, a frame corresponding to the average temperature, energy, and volume was selected and used to initiated a 1 ns NVE simulation for analysis, using the high frequency frame saving. This system is labelled *misfolded #1*. In the second procedure one frame corresponding to the average temperature and energy was selected from the high temperature run. Using this as an initial frame, a 100 ns simulation was performed at room temperature using a NPT simulation. From this simulation ten frames corresponding to the average energy and temperature and volume were selected, and from each, a 1 ns NVE run was conducted. This system is labelled *misfolded #2*. As the first quenching method is likely to produce a wider variety of structures than the second, comparing the misfolded system #1 and #2 allows checking whether variations in the misfolded quenched structure influence the final water dynamics. The ten 1 ns trajectories were subjected to dynamical analysis. We studied the misfolded

protein at ambient conditions rather than elevated temperature where the unfolding occurs, in order to keep the bulk water behavior as close as possible to the native state simulations, and focus entirely on the differences in dynamics induced by the altered protein surface.

## Analysis

### Hydrogen bond life times

For the rest of the article hydrogen bonds will be referred to as H-bonds. An H-bond was defined present if the distance between H-bond donor $D$ and acceptor atom $A$, $R_{DA} \leq 0.35$ nm, and the angle between the $DA$ and $DH$ vectors $\theta_{ADH} \leq 30\,^{\circ}$[21,22]. Here, either the donor and acceptor atom can belong to the protein or to water. The H-bond lifetime was defined as the time it takes for the bond to break and to form a stable bond with another acceptor (jump), or to remain dangling (translational diffusion/no jump). We identified a "jump" when the original O-H-A1 bond is broken and a new bond O-H-A2 is formed within $\Delta\tau$=200 fs. If the original bond O-H-A1 is broken but no new bond is formed within $\Delta\tau$=200 fs, the breaking process is classified as diffusive (no jump). The recrossing time $\Delta\tau$ = 200 fs was based on the fact that the vibrational characteristics of the water-water H-bond occur in the far infrared and around 200 $cm^{-1}$=166 fs[23,24]. Different values of this recrossing time $\Delta\tau$ = 0 fs and $\Delta\tau$ = 400 fs were used to test whether this choice affects the results.

### Water reorientation dynamics

Reorientation dynamics can be represented using the time correlation function[25,26]

$$C_2(t) = \frac{2}{5}\langle P_2[\mathbf{u}(0) \cdot \mathbf{u}(t)]\rangle, \tag{1}$$

where $P_2$ denotes the second Legendre polynomial, $\mathbf{u}$ is the unit vector characterizing the orientation of an OH group in a given frame and the angular brackets denote an ensemble average over all water molecules and all time origins. This correlation function can easily

be related to anisotropy curves obtained from polarization-resolved femtosecond infrared spectroscopy and to orientation relaxation times from magnetic relaxation techniques[25].

From MD simulations we compute the reorientation dynamics for each individual molecule. We are particularly interested in the anisotropy decay of water molecules hydrating different protein sites. The reorientation dynamics of individual water molecules was investigated by following the dynamics of both OH bond vectors of each molecule $j$. For each bond unit vector $\mathbf{u}_{jk}(t)$, we computed the time correlation function

$$c_j^m(t) = \frac{1}{5\ell} \sum_{t'=t_0^m}^{t_0^m+\ell\Delta t} \sum_{k=1}^{2} P_2[\mathbf{u}_{jk}(t')) \cdot \mathbf{u}_{jk}(t'+t))], \tag{2}$$

where the sum over $k = 1, 2$ refers to the two OH bond vectors, and the time correlation is summed over the $m$th time interval $t_0^m < t' < t_0^m + \ell\Delta t$ that the molecule is within the hydration layer of the protein (defined as the water oxygen being within 4.4 Å from the protein heavy atoms). We used a buffer time of 2 ps to avoid counting fast non-essential excursions inside and outside the hydration layer[27]. For each curve $c_j^m(t)$ we extracted the reorientation decay time $\tau_j^m$ by fitting $c_j^m(t)$ to a single exponential fit in the interval $0 < t < 10$ ps (see Fig S4 of the Supporting Information). Each estimate $m$ was viewed as a separate measurement, since the water molecule can change its dynamics when leaving or entering the hydration layer. For each water molecule $j$ and for each $m$th interval of length $\ell$ the decay time $\tau_j^m$ was histogrammed with a weight $\ell$, leading to a probability distribution of decay times. The weight $\ell$ follows from the fact that the correlation in Eq. 2 occurs $\ell$ times in Eq. 1. The average decay time $\tau$ from these histograms thus should be close to the overall decay time of Eq.1. The decay times of the individual water molecules allow us to establish the relation between the water structure and dynamics. We therefore divide the waters into several categories. For each water molecule $j$ and for each $m$th interval $\ell$ the decay time $\tau_j^m$ was histogrammed with a weight $\ell f_{HB}$ in the protein H-bonded category or with a weight $\ell f_{nHB}$ to the category of water that is non H-bonded to the protein. Here,

$f_{HB}$ and $f_{nHB}$ denote the fraction of frames in the interval $\ell$ in which water molecule $j$ was hydrogen bonded to the protein or not, respectively.

A similar procedure was followed for categorizing and histogramming hydrophobic or hydrophilic water. For each water molecule $j$, the decay time $\tau_j^m$ for each $m$th interval $\ell$ was histogrammed with a weight $\ell f_{HP}$ and $\ell f_{HF}$ for hydrophobic and hydrophilic water, respectively. Here $f_{HP}$ and $f_{HF}$ are the fraction of frames in the interval $\ell$ in which the water $j$ solvated respectively, a hydrophobic and hydrophilic group (i.e. the water oxygen was within 4.4 Å of, respectively an apolar or polar residue side chain). Note that this procedure implies that some water molecules can contribute to both categories. In both cases the sub-population histograms add up to the total probability histograms. Errors in the mean were estimated from block averaging.

## Polarization-resolved femtosecond infrared spectroscopy

Experimentally, we measured the water reorientation dynamics using polarization-resolved femtosecond infrared spectroscopy[9–11,24,28–30]. Protein solutions of 5, 10, 20 and 30% w/w were prepared by mixing bovine $\alpha-$lactalbumin (purity $>$ 90%, Davisco foods) with isotopically diluted water, consisting of ultrapure milli$-$Q grade $H_2O$ and 4% D2O (99.9%D, Cambridge Isotope Laboratories). The deuterated hydroxyl (OD) groups in this solution absorb strongly at 2500 cm$^{-1}$, which corresponds to the stretch vibration of the OD group.

We excited and probed the OD stretch vibrations using resonant infrared pulses. These pulses were generated by frequency conversion of the output of a Ti:sapphire regenerative amplifier that produces 850 $\mu$J, 100 femtosecond pulses with a center wavelength of 800 nm at a repetition rate of 1 kHz. Part of the light was used to pump a BBO$-$based optical parametric amplifier. The 2 $\mu$m idler pulses produced by this amplifier were frequency$-$doubled in another BBO crystal and subsequently mixed with the remaining 800 nm light in a lithiumniobate crystal, yielding 10 $\mu$J pulses at 2500 cm$^{-1}$, with a pulse duration of 200 fs and a bandwidth of 100 cm$^{-1}$. The pulse bandwidth largely covers the OD stretch absorption band,

such that the effects of spectral diffusion are negligible. These pulses were separated into pump, probe and reference beams by a wedged $CaF_2$ window and focused onto the sample by a parabolic mirror. The sample consisted of the protein solution sandwiched between two $CaF_2$ windows, held apart by a 50 $\mu$m spacer. After passing through the sample, the probe and reference beams were recollimated by a second parabolic mirror, dispersed in a grating-based spectrometer and detected with two lines of a 3x32 mercury−cadmium−telluride detector array.

The pump pulse induced transient absorption changes in the sample that we monitored with the probe pulse (the reference pulse was used for normalization to correct for pulse to pulse fluctuations of the infrared light). We measured the transient absorption for probe pulses with their polarization parallel and perpendicular with respect to the pump polarization. Since the pump pulse most efficiently excites OD vibrations with their transition dipole moment parallel to the polarization direction of the light, initially the parallel absorption signal is higher, while after some time the orientation of the OD stretch vibration has randomized, and the parallel and perpendicular signals become equal. From the parallel ($\alpha_{(\|)}$) and perpendicular ($\alpha_{\perp}$) transient absorption signals we constructed the anisotropy:

$$C_2(v,t) = \frac{\alpha_{(\|)}(v,t) - \alpha_{(\perp)}(v,t)}{(\alpha_{(\|)}(v,t) + 2\alpha_{(\perp)}(v,t))} \tag{3}$$

where $v$ denotes the frequency. The anisotropy $C_2(v,t)$ of Eq. 3 decays with the rate of molecular reorientation and is directly proportional to the second-order reorientation correlation function defined in Eq. 1. To compare the measured and computed anisotropy we average the experimental anisotropy over the OD frequency range $2450 - 2620\text{cm}^{-1}$.

# Results and Discussion

## Hydrogen bond dynamics

The computed H-bond life times for the six studied systems are shown in Table 1. The average and standard deviation are taken from a block average of 10 sets of data per system. Table S1 and S2 of Supporting Information show that, while the H-bond lifetime is sensitive to the selected recrossing time, the H-bond lifetimes follow the same trend when using different recrossing time $\Delta\tau$. We distinguish between water molecules that are H-bonded to other water molecules in the bulk, and water molecules that are donating or accepting H-bonds from the protein, as illustrated in Fig. 1. A protein H-bond donor leads in fact to two types of H-bonds, labelled the directD and D, with the first one being more informative about the direct protein water interaction, and the second one giving more relevant information on the reorientation of the OH vectors of the water accepting a H-bond from a protein donor (see Fig. 1 left). The H-bond type when the protein is accepting a hydrogen from water is labelled A (see Fig. 1 right). Table 1 shows that the overall average protein-water H-bond lifetime $t_{D+A}$ (the average over the H-bond lifetimes of bonds type A and D) is always longer than the H-bond lifetime in bulk water $t_{bulk}$ for all systems in this study, mainly due to bonds between accepting protein groups and water ($t_A$). The relative increase of the protein-water H-bond lifetimes at the protein surface can be expressed as the ratio $S_{HB}$ of the average protein-water H-bond lifetime over the average lifetime in the bulk (see Table 1). The protein-water H-bond lifetime distribution is broad, including short H-bonds but also long-lived bonds, as indicated by the long tail in Fig. S1 of the Supporting Information. The protein H-bond acceptors ($t_A$) form longer-lived bonds than the protein H-bond donating groups ($t_D$ and $t_{directD}$), which agrees well with the work of Sterpone et al[5,31] who showed that the water dynamics is slowed down more at protein H-bond accepting groups. Upon misfolding the protein-water H-bond lifetimes do not change much compared to the folded native state. However, the average lifetimes of H-bonds between protein donating groups and

water ($t_D$ and $t_{directD}$) increase upon misfolding, suggesting the existence of water mediated interactions between the protein residues in the misfolded systems, which are known to mediate folding of misfolded and unfolded systems[32]. Such a water mediated interaction is illustrated in Fig. S2 of the Supporting Information. The H-bond dynamics in the 5% TIP4P/2005 system is substantially slower compared to the 5% SPC/E system. The larger standard deviation of protein-water H-bond lifetimes upon misfolding is due to the different conformations in the ten analyzed windows of the misfolded system. The effect of protein concentration on the protein-water H-bond dynamics is marginal. Note that for the SPC/E system, the protein-water H-bond dynamics slightly decelerates with concentration, whereas it slightly accelerates for the TIP4P/2005 system.

To investigate the nature of the water-protein H-bond dynamics, we analyzed the H-bond breaking mechanism as a function of the protein site. For this process, Laage et al[33] introduced a framework involving large-amplitude angular jumps upon H-bond breakage. Figure 2 depicts the percentage of protein water H-bonds breaking via jumps as a function of the protein sites. This figure clearly shows a correlation between the curvature of the protein site (excluded volume) and the mechanism of H-bond breaking. For convex protein sites, protein water H-bonds break more likely via a jump mechanism, whereas for concave sites (occurring more in buried residues) H-bonds break via translational diffusion. This finding was also reported in the work of Brandeburgo et al[24], and can be rationalized by realizing that at concave sites there is less space for new hydrogen-bond partners, making it less likely that a water OH will find a new partner to jump to through an angular jump, thus increasing the chance of H-bonds breaking via diffusion.

## Reorientation dynamics

### Anisotropy decay of water

Figure 3 (left) shows for the six simulated systems the computed anisotropy decay averaged over all water molecules, as well as the experimental anisotropy decay curve for a 5% w/w pro-

tein solution, measured by polarization-resolved femtosecond infrared spectroscopy. While the computed anisotropy curves for SPC/E are systematically lower than the experimental one, their slope is very similar. As the hydration water comprises only 6% of the overall water in the simulation box, these decay curves are dominated by the reorientation time of bulk water. Figure 3 (right) shows the simulated anisotropy decay for water molecules that are initially in the hydration layer (within 4.4 Å of the protein heavy atoms). In accordance with the work of Sterpone et al. and Fogarty et al.[5,7], for all systems the decay time of the hydration shell anisotropy is longer compared to the corresponding overall water anisotropy decay of Fig. 3 (left). Thus, the water reorientation dynamics in the hydration shell of the protein is slowed down for all systems under study.

**Slow waters**

The anisotropy decay curve can be described at intermediate times ($0.5 < t < 7ps$) with the expression

$$C_2(t) = R_0 e^{-t/t_r} + R_1, \tag{4}$$

where the constant $R_1$ represents the water molecules in the hydration layer of the protein that reorient very slow ($t > 7$ ps), while most of the water molecules reorient with bulk-like reorientation time $t_r$. We limit our analysis to the first 7 ps of the anisotropy decay because the standard deviation in the ultrafast infrared experiments increases strongly with increasing delay time. Reducing the water content by increasing the concentration leaves $t_r$ more or less constant. For the simulations $t_r$ is $2.42 \pm 0.03$ and $2.40 \pm 0.02$ for 5% w/w SPC/E and 8.5% w/w SPC/E, respectively, close to the experimental value of bulk like water $t_r = 2.45 \pm 0.15$. The fraction of slow waters $f_{slow} = R_1/0.4$ (0.4 is the maximum value of the anisotropy) increases with the protein concentration, both in experiment and simulations. Figure 4 shows $f_{slow}$ as a function of protein concentration. The slope of the plot of $f_{slow}$ versus the concentration (in mol/kg water), multiplied with 55.25 ( mol water molecules per kg) then yields the number of slow waters per protein molecule. The experimental data yield

$323 \pm 16$ water molecules. For the SPC/E simulations, the number of slow water molecules is $350 \pm 33$. The SPC/E simulation data (bulk, 5% and 8.5%) in Fig. 4 fall within the error bars of the experimental values, and are hence in relatively good agreement with the experiment.

Analyzing the simulation results, we can also compute the amount of slow water molecules from the distribution of reorientation times as the fraction of the protein hydration shell water population reorienting slower than $\tau = 7$ ps (see Fig. 5 right). Multiplying this fraction with the average number of hydration waters gives the number of slow water molecules (per protein molecule since there is only one protein in the simulation box), which can again be compared with the experiment. For the 5 % SPC/E system the simulations yield $294 \pm 7$ slow water molecules, in fairly good agreement with the number of slow water found by experiments. The discrepancy between the two SPC/E estimates lies in the different ways of estimating the slow water content.

In contrast, for the 5% TIP4P/2005 system we find a higher number of slow water molecules compared to experimental findings. Calculating the number of slow water molecules from the slope of $f_{slow}$ and the reorientation time distribution we find $597 \pm 45$ and 519 slow water molecules, respectively. The slower dynamics of TIP4P/2005, is to be expected, since Vega et al[34] report a higher reorientation time for the TIP4P/2005 bulk water compared to the SPC/E bulk water by a factor of 1.2. The SPC/E model predicts the static dielectric constant better than TIP4P/2005[34] for the bulk water, therefore, it is expected to reproduce the experiments better.

### Triexponential fit of hydration water relaxation

As the experimental signal to noise ratio vanished for times larger than 7 ps and because the total anisotropy curve is dominated by bulk water relaxation, it does not make sense to fit to functions more complex than Eq. 4 to the experimental data. However, the situation is different for the hydration layer water molecules as calculated from the simulations. As these

waters are significantly slower than bulk water and experience a heterogeneous environment, it is worthwhile to fit the simulated hydration shell anisotropy decay (Fig. 3 bottom) to a triexponential function for times $0 < t < 70$ps:

$$C_2(t) = a_0 e^{-t/\tau_{r0}} + a_1 e^{-t/\tau_{r1}} + a_2 e^{-t/\tau_{r2}}, \tag{5}$$

with $a_0, a_1, a_2$ the amplitudes of the three exponential decay modes. There are three characteristic decay times a sub picosecond ($\tau_{r0}$): a moderate ($\tau_{r1}$) and a slow ($\tau_{r2}$) time scale. The sub-picosecond reorientation time is due to water libration modes, while the moderate and slow component indicate slower water reorientation mechanisms, dependent on the interaction with the protein. This observation agrees with the work of Brandeburgo et al.[24]. The relaxation times are larger for the TIP4P/2005 systems compared to the SPC/E systems, as shown in Table 2, Table 3 and Fig. 3. Note also that, upon misfolding, the moderate and slow characteristic time scales decrease, indicating a speed up of hydration water.

**Distribution of reorientation times**

The reorientation time of a water molecule clearly depends on its environment. This heterogeneity in the dynamics is visible in Fig. 5, which shows the probability distribution of the reorientation time $\tau$ for bulk water (Fig. 5 left), and for water molecules that are initially in the protein hydration layer (Fig. 5 right). The distribution for hydration water is much broader and extending toward longer reorientation times than the bulk water distribution (Fig. 5 left), which is roughly Gaussian, centered on 2.5 ps for SPC/E water and around 2.9 ps for TIP4P/2005 water. Note that the percentage of the hydration shell water reorienting slower than 100 ps is really small, less than 1.5% out of the overall hydration shell water. Fig. 6 visualizes the water reorientation time as function of protein site. It can be seen that some buried residues are hydrated by very slow internal waters, whereas at the surface, the water reorientation dynamics is relatively faster. As indicated above, water that is initially

H-bonded to the protein at concave sites is more confined and more likely to break its bond (type A or D) through translational diffusion[24]. Due to the reduced possibility to break the H-bond via a jump mechanism through a bifurcated hydrogen-bonded transition state, these water molecules reorient on longer timescales.

**Splitting the distributions**

Figure 5(right) shows the probability distribution for reorientation times of the hydration layer waters. These distributions are non-Gaussian due to the heterogeneous environments of the hydrating water molecules. In addition, bulk-like water still contributes to this distribution due to the definition of the hydration layer, and gives a peak at 2.5 ps, the characteristic reorientation time for bulk water. To obtain more insight in the origin of the heterogeneous reorientation time distribution in the hydration layer we categorize the water molecules based on their environment. For instance, we can subdivide the hydration water populations in hydrophobic and hydrophilic waters, based on the nearest protein residue (see Methods). Figure 7 (first column) and the first rows of Figures S5-S10 of the Supporting Information, show these distributions for different systems. Rather surprisingly, the hydrophilic and hydrophobic distributions do not show much difference in shape. This might be due to our weighting procedure (see Methods), which mixes the hydrophilic and hydrophobic categories to some extent. Table 3 reports the average reorientation time of the categories for all systems. For the native state systems, the hydrophobic water is slightly slower than hydrophilic water, possibly due to the fact that hydrophilic side groups are slightly more accessible to bulk-like water.

Another way we can categorize the water molecules is in terms of H-bonding to the protein. Figure 7 (right column) and the second rows of Figures S5-S10 of the Supporting Information show the distributions for this division for different systems. The water H-bonded to the protein is slower than the water that is not H-bonded to the protein. Note, that the latter category can be either hydrophobic or hydrophilic water which is not H-

bonded to the protein. The protein H-bonded water distribution exhibits a less pronounced bulk-like water peak, and has a long tail while the non protein H-bonded water has a larger contribution of bulk-like water. Table 3 shows that indeed the average reorientation time for the protein H-bonded waters ($\tau_{HB}$) in the native state is significantly longer than for the non protein H-bonded waters ($\tau_{nHB}$).

One can further subdivide the water molecules that are H-bonded to the protein into waters that donate their hydrogen to a protein acceptor (labeled $\mathrm{HB_{acc}}$) and waters that accept a bond from a protein donor (labeled $\mathrm{HB_{don}}$). As shown in Table 3 for all systems, water donating its hydrogen to a protein acceptor ($\tau_{HBacc}$ ) reorients slower compared to water that is accepting a hydrogen from a protein hydrogen donor ($\tau_{HBdon}$). This observation is in accordance with the results of Table 1 which showed that protein H-bond acceptor ($t_A$) form longer-living bonds than the protein hydrogen donating groups ($t_D$ and $t_{directD}$). We find that the strength of the H-bond, also plays a role in the reorientation dynamics, shown also by Usui et al[35]. Note that we average the reorientation dynamics of the two OH vectors to compute the reorientation time for each water molecule. Since the reorientation dynamics of the protein-bound OH group of a water molecule in the $\mathrm{HB_{acc}}$ category can be different from the dynamics of the other water OH group, we also compute the reorientation decay time $\tau_{HBacc'}$ of the single donated OH group. As expected, in all systems the protein-bound OH groups ($\tau_{HBacc'}$) exhibits a slower reorientation dynamics than the protein-bound water molecules (averaged over both OH vectors ($\tau_{HBacc}$)).

The curves in Fig 7 suggests three reorientation time regimes for the waters in the hydration shell, a bulk like regime (0-4 ps) peaked at 2.5 a moderately slow regime (4-20 ps) and a very slow regime ($>$ 20ps). Therefore we can also compare the different types of water based on their distribution over these time regimes. Table 4 shows the population (fraction) of hydration shell water molecules reorienting bulk-like, moderately slow or very slow according to its category: hydrophilic (HF), hydrophobic (HP), H-bonded to the protein (HB), non H-bonded to the protein (nHB), and finally all waters (all). While the hydropho-

bic/hydrophilic division hardly affects the fractions, clearly the waters that are H-bonded show a significantly larger fraction in the slow category, as expected. Again, TIP4P/2005 shows a slower behavior than SPC/E. Note that upon increasing the protein concentration (reducing the bulk water) for both SPC/E and TIP4P/2005 system, the hydration shell water reorients on average the same (see Table 3).

**Correlation of reorientation time with H-bond coordination number**

The dynamical heterogeneity of the protein hydration water is also observable experimentally. Fig 8 shows the measured anisotropy decay as a function of frequency at different picosecond delay times. For bulk water, the anisotropy decay is independent of frequency; but for water in $\alpha$-lactalbumin solutions the anisotropy decay becomes frequency dependent, with a slower decay on the high frequency side. As the frequency of the OD vibration depends on the H-bond strength, with strong H-bonds corresponding to low OD frequencies and weak H-bonds corresponding to high OD frequencies, this plot shows that water molecules with weaker H-bonds (high frequencies) reorient slower. This frequency dependence is not observed for small amphiphilic solutes[13,32], and therefore likely originates from the protein structure. This is consistent with the observation that the slowest reorienting waters are located in concave sites on the structured protein surface (Fig. 6). It also suggests that there is a correlation between the position of a water molecule at the protein surface and its H-bond strength. To further investigate this, we analyze the water H-bond coordination in the protein solutions, which directly influences the frequency of the OD stretch vibration[36].

Recently, Auer and Skinner[36] used Raman and VSF spectroscopy experiments to classify molecules in terms of H-bond structure in bulk and at a liquid vapor interface. In particular, they classified each water molecule by its number of H-bond acceptor $n_A$ and donors $n_D$. Here we adopt this classification of the H-bond structure, using a slightly different notation ($n_A$-$n_D$), where $n_A$ is the number of accepted H-bonds, and $n_D$ the number of donated H-bonds (see Fig. 9 (a) for an illustration). Note that these numbers include bonds accepted

from and donated to the protein. For bulk water, the population of the different H-bond classes was found to decrease in the order (2-2) > (1-2) > (2-1) > (1-1) > (0-2). Our simulations show the same order for bulk water in the different protein systems (see Fig. 9 and Fig. S3 of Supporting Information). We find the average number of H-bonds of bulk water to be 3.54 and 3.62 for SPC/E 5% and 8.5%, respectively, in accordance with reported values of 3.59 for SPC/E water[37]. Fig. 9 (b) shows that near a protein water interface, in this case for the 5% SPC/E system, the water H-bond class population decreases in the order $(2-2) > (1-2) > (2-1) > (1-1) > (0-2)$, which is the same as for bulk water. However, comparing protein hydration shell water with bulk water the populations $(1-2)$ and $(1-1)$ are enhanced and $(2-1)$ and $(2-2)$ are reduced in the hydration shell. This shift leads to an average of 3.31 H-bonds for the hydration shell water, which is less compared to bulk water (3.59 H-bonds). Similar results are found for the 5 % TIP4P/2005, misfolded #1 and misfolded #2 systems with average H-bond numbers of 3.43, 3.29 and 3.29, respectively.

To relate the contribution from each of the H-bond classes to the water reorientation time distributions we partitioned these distributions based on the coordination labels ($n_A$-$n_D$). The resulting distributions are shown in Fig. 9 (c) and Figures S5-S10 of the Supporting Information. The H-bond class of a water molecule does not seem to have a dramatic effect on the reorientation time distribution. To see the difference more clearly in Fig. 9 (d) we separate for the 5% SPC/E system the distributions for the different populations into three reorientation time regimes: a bulk like (0-4 ps) peaked at 2.5, a moderately slow (4-20 ps ) and a very slow (> 20ps). Even though the populations themselves are widely spread, there is a clear correlation in this table: water with more donated H-bonds are slower, waters with more accepted H-bonds faster (increased bulk like population). This pattern occurs in all hydration water, but not in bulk, where there is no correlation between the water structures and the dynamics. This correlation is made even clearer in Table 5 which shows the fraction of water as a function of number of donated and accepted H-bonds, irrespective of class. The correlation however, does not mean causation. Much more likely, the presence of the

surface induces both effects: fewer accepted H-bonds, and slower reorientation dynamics.

**Effect of misfolding on reorientation dynamics**

High temperature simulations indicated a loss of secondary and tertiary structure in $\alpha$-lactalbumin, breaking of hydrogen bonds and exposure of hydrophobic groups to the solvent. Lowering the temperature again did not result in refolded structures, but rather in a collapsed structure without any secondary or tertiary structure. Figure S11 in the Supporting Information shows the structural changes in terms of the root-mean-square-deviation (RMSD) with respect to the native state, the total solvent accessible surface area (SASA), and the SASA of the hydrophobic and hydrophilic groups. As expected misfolded structures have a larger RMSD, an enhanced SASA, and increased hydrophobic area. Note that the two misfolded systems show quite similar trends, with the main difference that misfolded #1 shows a broader distribution, reflecting a wider variety of structures.

There seems to be a negligible difference between the two types of misfolded systems in terms of the reorientation decay times, as the average $\tau$ values given in Table 3 are similar and the anisotropy decay curves in Fig. 3 are identical within the error. This suggests that the type of quenching procedure does not influence the hydration water reorientation dynamics, and that the precise details of the misfolded structures are only of secondary importance. Nevertheless, the hydration shell water reorientation time of the unfolded structures is faster compared to the native structure (see Table 2, 3 and Fig. 3b). This is in accordance with the work of Jose *et al.*[12] who showed that the disordered A$\beta_{1-42}$ amyloid protein exhibits faster water reorientation dynamics than a globular ubiquitin protein.

From the distributions of Figure 7 and S8, the calculated number of slow water molecules for the misfolded systems are 373 and 401 for misfolded #1 and misfolded #2, respectively, higher than for the native 5% SPC/E system. This increase in the number of slow waters is due to the larger solvent accessible surface of a misfolded protein, with respect to the native state, as also shown in Fig. S11 of the Supporting information. This also follows from

Fig. 7 which compares the number distributions for the native and misfolded protein as a function of decay time $\tau$ for surface waters near hydrophobic/hydrophilic groups. Similar to the native state results, both hydrophobic and hydrophilic water have a bulk like peak around 2.5 ps for the misfolded conformations. The largest difference between the native and misfolded state is the enhanced contribution of hydrophobic hydration water in the misfolded state. Not surprisingly, misfolding induces more hydrophobic residues to be exposed.

Table 4 compares the fraction of the bulk-like, moderate and slow hydration shell waters of the native and misfolded systems. The hydrophobic water in the misfolded systems exhibits a higher fraction of bulk-like water and a lower fraction of moderate and slow water compared to the native systems, and indeed, a smaller average reorientation decay time for the hydrophobic water (see Table 3 ). Interestingly, not only the water dynamics accelerates upon misfolding, but the hydrophobic water becomes actually slightly faster compared to the hydrophilic water. This larger fraction of non surface-perturbed waters was also observed in the work of Rahaman et al[13].

The contribution of water not H-bonded to the protein (nHB) to the decay time distributions in Fig. 7 and S5-S10 of the Supporting Information is significantly higher for the misfolded state than for the native state. At the same time the contribution of water H-bonded to the protein (HB) only increases slightly between the native and misfolded state. This increased population of water non-H-bonded to the protein represents to a large extent the higher hydrophobic water population and similarly shows a slightly faster reorientation.

Table 2 and 3 show that the average hydration layer water in the misfolded state tends to be faster than in the native states. Water that is H-bonded to the protein remains slower than the water non-H-bonded to the protein, and as in the native systems, shows a less pronounced bulk-like peak. The H-bonded water is slightly faster in the misfolded state, unlike the H-bond lifetimes that remain unchanged. This suggests the strength of the bond does not change upon misfolding, but rather the decreased local excluded volume upon misfolding causes water to reorient faster (more bulk-like).

Interestingly, upon misfolding water that accepts a H-bond from a protein donor slightly slows down (see Table 3). In accordance with the increase of the protein donor – water H-bond lifetime ($t_D$, $t_{Direct}$) upon misfolding this bond does become stronger and therefore water reorients slower. This can be explained by the presence of water mediated H-bonds in a misfolded state (see Fig. S2 of the Supporting Information for an illustration). Fig. 6 shows projections of the water reorientation time on structural representations of the protein. Finally, Figures S5-S10 of the Supporting Information shows that misfolding does not change the order of the population of H-bonding classes, but again that hydrophobic groups become more solvent accessible.

# Conclusions

Using ultrafast IR spectroscopy experiments and molecular dynamics simulations we investigated the dynamics of hydration water in $\alpha$-lactalbumin solutions. We found good agreement between simulation and experiment for the number of slow waters around the protein surface. The simulations showed that the slowly reorienting water molecules are hydration shell waters that make on average fewer H-bonds with the surrounding molecules in comparison to bulk water. The slowest water molecules are those that do not accept H-bonds from other water molecules or protein residues, and that donate two hydrogen bonds to the protein. The water near the hydrophobic groups of the protein exhibits on average slightly slower reorientation dynamics than the water near the hydrophylic groups. These conclusions are corroborated by femtosecond mid-infrared spectroscopic measurements. In the experiment the hydration shell water molecules are recognized from the fact that they are involved in less and weaker hydrogen bonds compared to bulk water. These water molecules are observed to show much slower reorientation dynamics than bulk water.

The H-bond breaking mechanism is also affected. Near convex sites the jump process dominates the breaking procedure, while near concave sites jumping becomes less frequent,

thus slowing down the reorientation of water molecules. At concave sites the diffusive process (without jumps) becomes relatively more important.

Upon misfolding a larger amount of water reorients slowly, mainly due to the increase of the solvent accessible surface. However, the hydration shell water dynamics slightly accelerates compared to the native hydration shell water, due to an increased fraction of bulk-like waters near hydrophobic groups. In the misfolded systems, the hydrophobic residues are more exposed to the bulk and are no longer part of a concave protein cavity. As a result, the reorientation of water molecules near hydrophobic groups becomes relatively faster compared to the folded systems. The protein-water H-bond lifetime does not change significantly upon misfolding, although waters accepting a H-bond from a protein donor reorient slower, probably due to water mediated protein interactions.

## Associated content

Supporting Information available: average water hydrogen bond lifetimes, bulk water reorientation time distributions, hydration shell water reorientation distributions, snapshot of water-mediated protein interaction, structural analysis of misfolded states .This material is available free of charge via the Internet at http://pubs.acs.org

## Acknowledgement

This work is supported by NanoNextNL, a micro and nanotechnology consortium of the Government of the Netherlands and 130 partners. We acknowledge support from the Nederlandse Organisatie voor Wetenschappelijk Onderzoek (NWO) for the use of supercomputer facilities. WHB contributed to this work only during this employment at the University of Amsterdam.

## References


(1) Bandyopadhyay, S.; Chakraborty, S.; Bagchi, B. Secondary Structure Sensitivity of Hydrogen Bond Lifetime Dynamics in the Protein Hydration Layer. *J. Am. Chem. Soc.* **2005**, *127*, 16660–7.

(2) Eppler, R. K.; Komor, R. S.; Huynh, J.; Dordick, J. S.; Reimer, J. A.; Clark, D. S. Water Dynamics and Salt-Activation of Enzymes in Organic Media: Mechanistic Implications Revealed by NMR Spectroscopy. *Proc. Natl. Acad. Sci. U.S.A.* **2006**, *103*, 5706–5710.

(3) Grossman, M.; Born, B.; Heyden, M.; Tworowski, D.; Fields, G. B.; Sagi, I.; Havenith, M. Correlated Structural Kinetics and Retarded Solvent Dynamics at the Metalloprotease Active Site. *Nat. Struct. Mol. Biol.* **2011**, *18*, 1102–8.

(4) Kiihne, S.; Bryant, R. G. Protein-Bound Water Molecule Counting by Resolution of 1H Spin-Lattice Relaxation Mechanisms. *Biophys. J.* **2000**, *78*, 2163–2169.

(5) Sterpone, F.; Stirnemann, G.; Laage, D. Magnitude and Molecular Origin of Water Slowdown Next to a Protein. *J. Am. Chem. Soc.* **2012**, *134*, 4116–9.

(6) Li, T.; Hassanali, A. A.; Kao, Y.T.; Zhong, D.; Singer, S. J. Hydration Dynamics and Time Scales of Coupled Water – Protein Fluctuations. *J. Am. Chem. Soc.* **2007**, *129*, 3376–3382.

(7) Fogarty, Aoife C and Laage, D. Water Dynamics in Protein Hydration Shells: the Molecular Origins of the Dynamical Perturbation. *J. Phys. Chem. B* **2014**, *118*, 7715–7729.

(8) Halle, B. Protein Hydration Dynamics in Solution: a Critical Survey. *Philos Trans R Soc Lond B Biol Sci* **2004**, *359*, 1207–23; discussion 1223–4, 1323–8.

(9) Dokter, A. M.; Woutersen, S.; Bakker, H. J. Inhomogeneous Dynamics in Confined Water Nanodroplets. *Proc. Natl. Acad. Sci. U.S.A.* **2006**, *103*, 15355–15358.

(10) Fenn, E. E.; Wong, D. B.; Fayer, M. D. Water Dynamics at Neutral and Ionic Interfaces. *Proc. Natl. Acad. Sci. U.S.A.* **2009**, *106*, 15243–15248.

(11) Bakulin, A. A.; Pshenichnikov, M. S.; Bakker, H. J.; Petersen, C. Hydrophobic Molecules Slow Down the Hydrogen-Bond Dynamics of Water. *J. Phys. Chem. A* **2011**, *115*, 1821–1829.

(12) Jose, J. C.; Khatua, P.; Bansal, N.; Sengupta, N.; Bandyopadhyay, S. Microscopic Hydration Properties of the Aβ1–42 Peptide Monomer and the Globular Protein Ubiquitin: a Comparative Molecular Dynamics Study. *J. Phys. Chem. B* **2014**, *118*, 11591–11604.

(13) Rahaman, O.; Melchionna, S.; Laage, D.; Sterpone, F. The Effect of Protein Composition on Hydration Dynamics. *Phys. Chem. Chem. Phys* **2013**, *15*, 3570–6.

(14) Markus, C. R.; Olivier, B.; Panhuysen, G. E. M.; Gugten, J. V. D.; Alles, M. S.; Tuiten, A.; Westenberg, H. G. M.; Fekkes, D.; Koppeschaar, H. F.;de Haan, E. H.F The Bovine Protein α-Lactalbumin Increases the Plasma Ratio of Tryptophan to the Other Large Neutral Amino Acids , and in Vulnerable Subjects Raises Brain Serotonin Activity , Reduces Cortisol Concentration , and Improves Mood Under Stress. *Am J Clin Nutr* **2000**, *71*, 1536–1544.

(15) Halskau, O. y.; Perez-jimenez, R.; Ibarra-molero, B.; Underhaug, J.; Mun, V.; Martinez, A.; Sanchez-ruiz, J. M. Large-Scale Modulation of Thermodynamic Protein Folding Barriers Linked to Electrostatics. *Proc. Natl. Acad. Sci. U.S.A.* **2008**, *105*, 8625.

(16) Pronk, S.; Páll, S.; Schulz, R.; Larsson, P.; Bjelkmar, P.; Apostolov, R.; Shirts, M. R.; Smith, J. C.; Kasson, et al; GROMACS 4.5: a High-Throughput and Highly Parallel Open Source Molecular Simulation Toolkit. *Bioinformatics (Oxford, England)* **2013**, *29*, 845–54.

(17) Chrysina, E. D.; Brew, K.; Acharya, K. R. Crystal Structures of Apo and Holo-Bovine

Alpha-Lactalbumin at 2.2 Å Resolution Reveal an Effect of Calcium on Inter-Lobe Interactions. *J. Biol. Chem.* **2000**, *275*, 37021–37029.

(18) Lindorff-Larsen, K.; Piana, S.; Palmo, K.; Maragakis, P.; Klepeis, J. L.; Dror, R. O.; Shaw, D. E. Improved Side-Chain Torsion Potentials for The Amber ff99SB Protein Force Field. *Proteins* **2010**, *78*, 1950–8.

(19) Bussi, G.; Donadio, D.; Parrinello, M. Canonical Sampling Through Velocity Rescaling. *J. Chem. Phys.* **2007**, *126*, 014101.

(20) Parrinello, M. Polymorphic Transitions in Single Crystals: a New Molecular Dynamics Method. *Journal of Applied Physics* **1981**, *52*, 7182.

(21) Lin, I-C.; Seitsonen, A.; Tavernelli, I.; Rothlisberger, U. Structure and Dynamics of Liquid Water from ab Initio Molecular Dynamics Comparison of BLYP, PBE, and revPBE Density Functionals with and without van der Waals Corrections. *J. Chem. Theory Comput.* **2012**, *8*, 3902–3910.

(22) Berendsen, H. J. C.; Postma, J. P. M.; Van Gunsteren, W. F.; Hermans, J. Intermolecular Forces, ed Pullman B. **1981**.

(23) Brubach, J.-B.; Mermet, A.; Filabozzi, A.; Gerschel, A.; Roy, P. Signatures of the Hydrogen Bonding in the Infrared Bands of Water. *J. Chem. Phys.* **2005**, *122*, 184509.

(24) Brandeburgo, W. H.; Post, T. V. D.; Meijer, J. On the Slowdown Mechanism of Water Dynamics Around Small Amphiphiles. *Phys. Chem. Chem. Phys.* **2015**, *17*, 24968.

(25) Bakker, H. J.; Skinner, J. L. Vibrational Spectroscopy as a Probe of Structure and Dynamics in Liquid Water. *Chem Rev* **2010**, *110*, 1498–517.

(26) Lipari, G.; Szabo, A. Effect of Librational Motion on Fluorescence Depolarization and Nuclear Magnetic Resonance Relaxation in Macromolecules and Membranes. *Biophys. J.* **1980**, *30*, 489–506.

(27) Massi, F.; Straub, J. E. Structural and Dynamical Analysis of the Hydration of the Alzheimer's $\beta$-Amyloid Peptide. *J. Comput. Chem.* **2003**, *24*, 143–153.

(28) Rezus, Y.; Bakker, H. Observation of Immobilized Water Molecules Around Hydrophobic Groups. *Phys Rev Lett* **2007**, *99*, 148301.

(29) van der Loop, T. H.; Panman, M. R.; Lotze, S.; Zhang, J.; Vad, T.; Bakker, H. J.; Sager, W. F. C.; Woutersen, S. Structure and Dynamics of Water in Nonionic Reverse Micelles: a Combined Time-Resolved Infrared and Small Angle X-Ray Scattering Study. *J. Chem. Phys.* **2012**, *137*, 044503.

(30) van der Post, S. T.; Bakker, H. J. The Combined Effect of Cations and Anions on the Dynamics of Water. *Phys. Chem. Chem. Phys.* **2012**, *14*, 6280–8.

(31) Sterpone, F.; Stirnemann, G.; Hynes, J. T.; Laage, D. Water Hydrogen-Bond Dynamics Around Amino Acids: the Key Role of Hydrophilic Hydrogen-Bond acceptor groups. *J. Phys. Chem. B.* **2010**, *114*, 2083–9.

(32) Pabón, G.; Amzel, L. M. Unfolding Ubiquitin by Force : Water mediated H-bond Destabilization. *Universitas Scientiarum* **2012**, *17*, 273–281.

(33) Laage, D.; Hynes, J. T. A Molecular Jump Mechanism of Water Reorientation. *Science (New York, N.Y.)* **2006**, *311*, 832–5.

(34) Vega, C.; Abascal, J. L. F. Simulating Water With Rigid Non-Polarizable Models: a General Perspective. *Phys. Chem. Chem. Phys* **2011**, *13*, 19663–88.

(35) Usui, K.; Hunger, J.; Sulpizi, M.; Ohto, T.; Bonn, M.; Nagata, Y. Ab Initio Liquid Water Dynamics in Aqueous TMAO Solution. *J. Phys. Chem. B.* **2015**, *119*, 10597–606.

(36) Auer, B.; Skinner, J. Water: Hydrogen Bonding and Vibrational Spectroscopy, in the Bulk Liquid and at the Liquid/Vapor Interface. *Chem. Phys. Lett.* **2009**, *470*, 13–20.

(37) Xu, H.; Stern, H.; Berne, B. Can Water Polarizability be Ignored in Hydrogen Bond Kinetics? *J. Phys. Chem. B.* **2002**, *25*, 2054–2060.

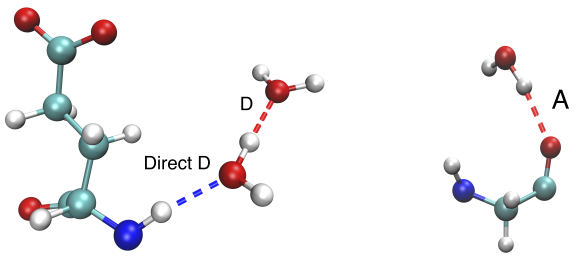


Figure 1: Representation of the H-bond type. Left: a protein donating a H-bond to water, labelled directD and the accepting water donating a H-bond to another water labelled D. Right: a protein accepting a H-bond from water, labelled A. The classification includes both backbone and side-chain H-bonds.

**Table 1: Simulation: Average protein water and bulk water H-bond lifetimes for six different systems 1) 5% protein in SPC/E water 2) 8.5% protein in SPC/E water 3) misfolded #1 4) misfolded #2 5) 5% protein in TIP4P/2005 water 6) 8.5% protein in TIP4P/2005 water. The subscript indicates the error in the last digit(s).**

| system # | 1 | 2 | 3 | 4 | 5 | 6 |
|---|---|---|---|---|---|---|
| $t_{bulk}$ | $2.45_1$ | $2.47_1$ | $2.45_1$ | $2.47_1$ | $2.90_1$ | $2.95_1$ |
| $t_D$ | $3.27_5$ | $3.41_{13}$ | $3.43_7$ | $3.61_{15}$ | $3.93_5$ | $3.84_5$ |
| $t_A$ | $4.62_9$ | $4.70_{14}$ | $4.53_{15}$ | $4.67_{13}$ | $5.72_{10}$ | $5.61_{21}$ |
| $t_{D+A}$ | $3.99_6$ | $4.23_{14}$ | $4.01_{14}$ | $4.17_{14}$ | $4.84_7$ | $4.74_7$ |
| $t_{directD}$ | $1.99_5$ | $1.53_5$ | $2.15_2$ | $2.14_5$ | $1.97_5$ | $1.88_3$ |
| $S_{HB}$ | 1.62 | 1.71 | 1.63 | 1.69 | 1.67 | 1.60 |

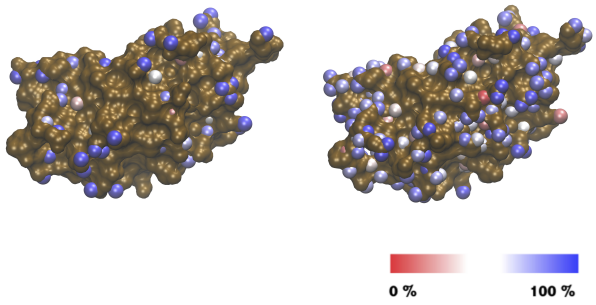


Figure 2: Simulation: Percentage of occurrence of jump mechanism of protein-water H-bond breaking projected on protein atoms. Left: type D, H-bonds. Right: type A, H-bond. Blue sites indicate that 100% of the H-bonds break via a jump mechanism, while red represents breaking through diffusion. Ochre sites do not form protein water H-bonds.

**Table 2: Simulation: Fit of the anisotropy curve for the hydration shell water population to a sum of three exponentials (Eq 5) for the six systems: 1) 5% SPC/E 2) 8.5% SPC/E 3) misfolded #1 4) misfolded #2 5) 5% TIP4P/2005 6) 8.5% TIP4P/2005. The subscript indicates the error in the last digit(s).**

| system # | 1 | 2 | 3 | 4 | 5 | 6 |
|---|---|---|---|---|---|---|
| $\tau_{r0}$ | $0.20_1$ | $0.20_1$ | $0.19_1$ | $0.18_1$ | $0.21_1$ | $0.19_1$ |
| $\tau_{r1}$ | $4.56_3$ | $4.60_4$ | $4.39_3$ | $4.41_3$ | $5.47_4$ | $5.34_4$ |
| $\tau_{r2}$ | $41.08_{55}$ | $40.8_{56}$ | $35.12_{51}$ | $34.44_{46}$ | $45.35_{63}$ | $40.20_{46}$ |

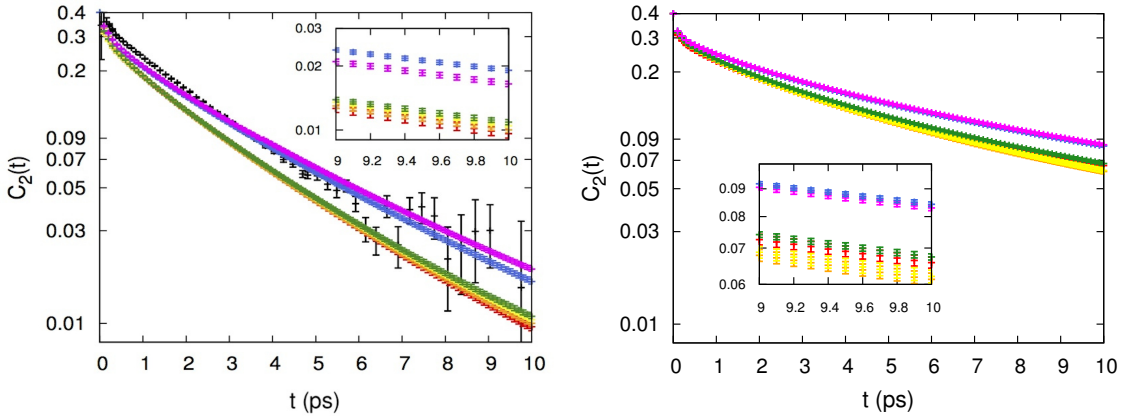


Figure 3: Left: Logarithmic plot of the anisotropy decay of all water molecules for the six simulated systems. Right : Anisotropy decay for hydration layer only. 5% SPC/E (red), 8.5% SPC/E (dark green),misfolded #1 (orange), misfolded #2 (yellow),5% TIP4P/2005 (blue), 8.5% TIP4P/2005 (magenta). Experimental anisotropy decay for a 5%wt protein solution, averaged over the frequency range 2450-2620 $cm^{-1}$ (black).

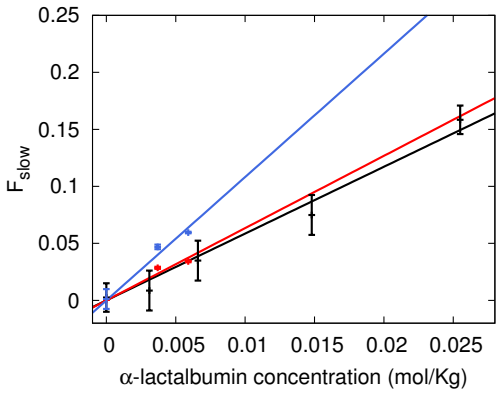


Figure 4: Fraction of slow water molecules as a function of $\alpha$-lactalbumin concentration: TIP4P/2005 system (blue), SPC/E system (red), fs-IR experiments (black). Lines are linear fits to the data points.

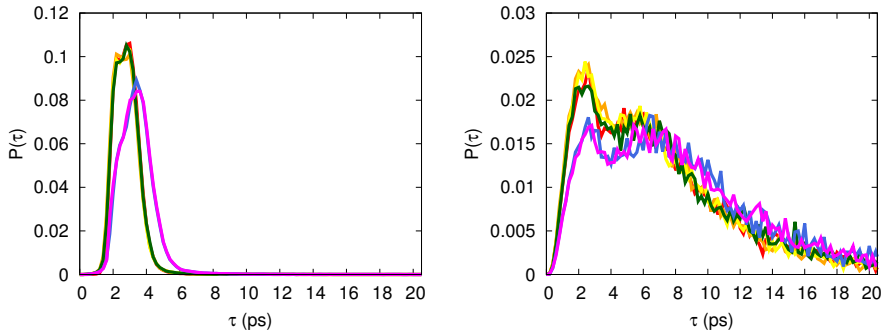


Figure 5: Simulation:probability distribution of reorientation decay $\tau$ of water molecules based on a geometrical ensemble, initially outside of the hydration shell (left) and initially in the hydration shell (right), for the six systems: 5% SPC/E (red), 8.5% SPC/E (dark green), misfolded #1 (orange), misfolded #2 (yellow), 5% TIP4P/2005 (blue), 8.5% TIP4P/2005 (magenta).

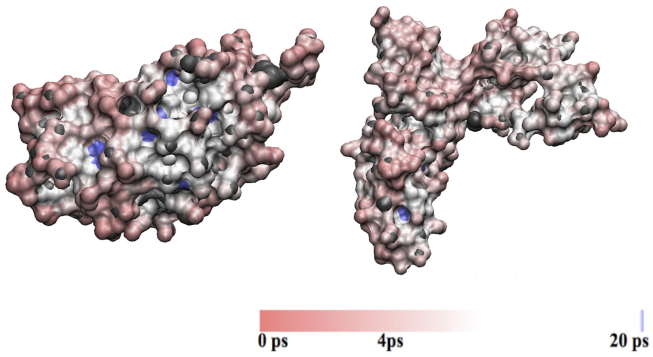


Figure 6: Simulation: The water reorientation decay times and the nature of the heavy atoms projected on protein surface for the two systems a) 5% SPC/E, (top) b) misfolded #1 (bottom). Red indicates fast water reorientation, white moderate, and blue slow. Grey indicates no water population close to that site. Note that the misfolded configuration has fewer blue sites, indicating relatively faster water reorientation.

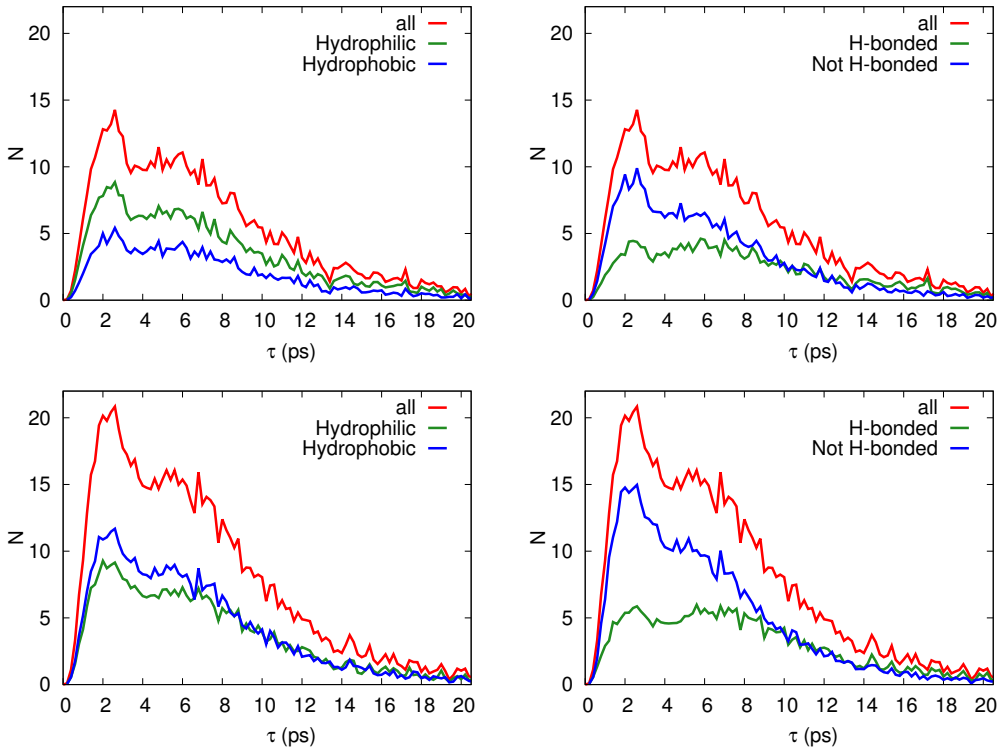


Figure 7: Simulation: Number distributions of reorientation decay times of the hydration water for 5% SPC/E (top row) and misfolded #1 (bottom row). The left column depicts the overall hydration water (red), and its subdivision into molecules hydrating hydrophilic (green) and hydrophobic (blue) groups. The right column depicts the overall hydration water (red), and its subdivision into molecules that are H-bonded to the protein (green) and molecules that are non H-bonded to the protein (blue).

**Table 3: Simulation: Reorientation decay time $\tau$ of water molecules in ps, based on its category for the six systems of study 1) 5% SPC/E 2) 8.5% SPC/E 3) misfolded #1 4) misfolded #2 5) 5% TIP4P/2005 6) 8.5% TIP4P/2005. The subscript indicates the error in the last digit(s).**

| system # | 1 | 2 | 3 | 4 | 5 | 6 |
|---|---|---|---|---|---|---|
| $\tau_{prot}$ | $4.07_5$ | $4.07_4$ | $3.85_9$ | $3.92_6$ | $4.93_6$ | $5.00_6$ |
| $\tau_{HF}$ | $4.02_3$ | $4.05_5$ | $3.98_{20}$ | $4.09_{15}$ | $4.80_3$ | $4.89_5$ |
| $\tau_{HP}$ | $4.17_9$ | $4.09_4$ | $3.75_7$ | $3.79_3$ | $5.17_{10}$ | $5.22_{16}$ |
| $\tau_{HB}$ | $5.05_9$ | $5.50_{26}$ | $4.66_{15}$ | $4.91_{20}$ | $6.23_{11}$ | $6.33_{17}$ |
| $\tau_{nHB}$ | $3.53_5$ | $3.53_2$ | $3.45_8$ | $3.48_6$ | $4.22_8$ | $4.31_6$ |
| $\tau_{HBacc}$ | $5.73_{15}$ | $5.98_{26}$ | $5.48_{22}$ | $5.69_{26}$ | $7.21_{14}$ | $7.37_8$ |
| $\tau_{HBacc'}$ | $6.32_{21}$ | $6.62_{31}$ | $5.88_{38}$ | $6.15_2$ | $8.25_{16}$ | $8.21_{26}$ |
| $\tau_{HBdon}$ | $4.25_{14}$ | $4.65_{19}$ | $4.42_{23}$ | $4.74_{32}$ | $5.11_4$ | $5.09_{28}$ |

**Table 4: Simulation: Fraction of hydration shell type of water molecules reorienting bulk-like ($\tau < 4ps$) , moderately slow ($4 \leqslant \tau < 20ps$) or very slow ($\tau \geqslant 20$).**

| | type | $\tau < 4ps$ | $4 \leqslant \tau < 20ps$ | $\tau \geqslant 20$ |
|---|---|---|---|---|
| 5% SPC/E | HF | 0.28 | 0.65 | 0.07 |
| | HP | 0.28 | 0.64 | 0.08 |
| | HB | 0.17 | 0.69 | 0.14 |
| | nHB | 0.35 | 0.62 | 0.03 |
| | all | 0.28 | 0.64 | 0.08 |
| 8.5 % SPC/E | HF | 0.28 | 0.65 | 0.07 |
| | HP | 0.30 | 0.62 | 0.08 |
| | HB | 0.18 | 0.67 | 0.15 |
| | nHB | 0.35 | 0.62 | 0.03 |
| | all | 0.29 | 0.64 | 0.07 |
| misfolded #1 | HF | 0.28 | 0.65 | 0.07 |
| | HP | 0.33 | 0.63 | 0.06 |
| | HB | 0.17 | 0.70 | 0.13 |
| | nHB | 0.34 | 0.63 | 0.03 |
| | all | 0.31 | 0.63 | 0.06 |
| misfolded #2 | HF | 0.28 | 0.65 | 0.07 |
| | HP | 0.32 | 0.62 | 0.06 |
| | HB | 0.21 | 0.67 | 0.12 |
| | nHB | 0.36 | 0.61 | 0.03 |
| | all | 0.30 | 0.63 | 0.07 |
| 5% TIP4P/2005 | HF | 0.22 | 0.69 | 0.09 |
| | HP | 0.20 | 0.69 | 0.1 |
| | HB | 0.14 | 0.69 | 0.17 |
| | nHB | 0.28 | 0.68 | 0.04 |
| | all | 0.21 | 0.69 | 0.10 |
| 8.5% TIP4P/2005 | HF | 0.21 | 0.68 | 0.11 |
| | HP | 0.20 | 0.69 | 0.11 |
| | HB | 0.14 | 0.69 | 0.17 |
| | nHB | 0.26 | 0.69 | 0.05 |
| | all | 0.21 | 0.69 | 0.10 |

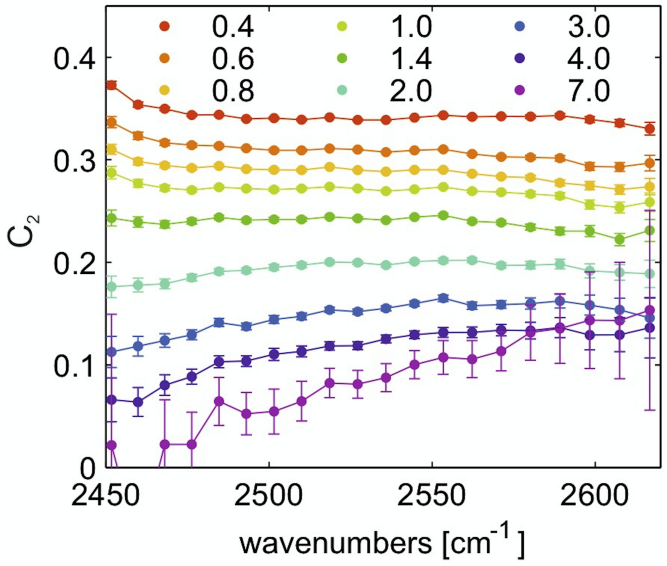


Figure 8: Experiment: Anisotropy decay for 30%w/w $\alpha$-lactalbumin in isotopically diluted water as a function of frequency at different picosecond delay times (indicated in the legend).

**Table 5: Simulation: Fraction of waters in hydration shell reorienting bulk-like ($\tau < 4ps$) , moderately slow ($4 \leqslant \tau < 20ps$) or very slow ($\tau \geqslant 20$ ) as function number of donated and accepted H-bonds.**

| # donated h-bonds | $\tau < 4ps$ | $4 \leqslant \tau < 20ps$ | $\tau \geqslant 20$ |
|---|---|---|---|
| 0 | 0.37 | 0.59 | 0.04 |
| 1 | 0.32 | 0.62 | 0.06 |
| 2 | 0.27 | 0.65 | 0.08 |
| # accepted h-bonds | $\tau < 4ps$ | $4 \leqslant \tau < 20ps$ | $\tau \geqslant 20$ |
| 0 | 0.20 | 0.64 | 0.16 |
| 1 | 0.28 | 0.64 | 0.08 |
| 2 | 0.30 | 0.64 | 0.06 |

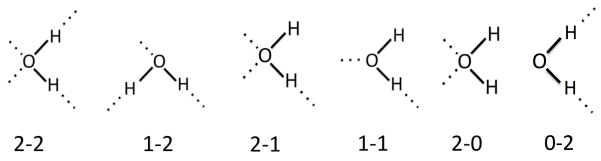


(a)

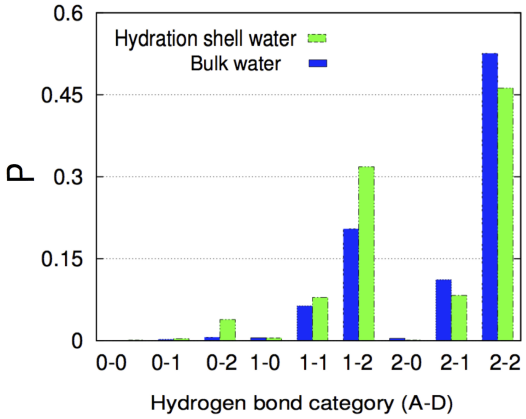


(b)

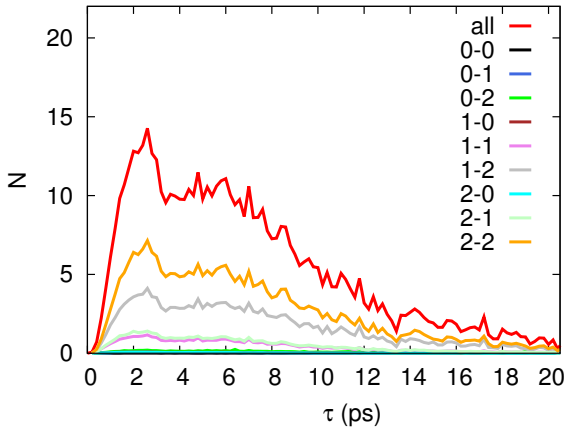


(c)

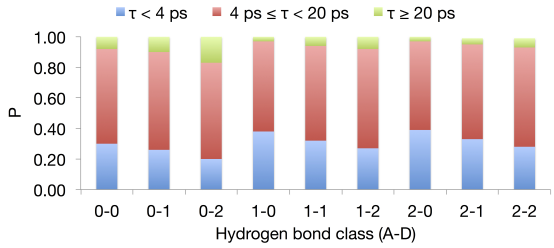


(d)

Figure 9: Simulation: a) Illustration of H-bond classes b) Populations of each H-bond class, subdivided into bulk and hydration shell water (for the 5% SPC/E system). c) Number distribution of the reorientation decay times of hydration shell water for the different H-bond classes (for the 5% SPC/E system). d) Percentage of water reorienting in the bulk-like (blue), moderate (red) and slow (green) regime for the different H-bond classes (for the 5% SPC/E system).